Turkish Journal of Electrical Engineering & Computer Sciences

http://journals.tubitak.gov.tr/elektrik/

Research Article

Turk J Elec Eng & Comp Sci
(2023) 31: 360 – 380

doi:10.55730/1300-0632.3989

Teamwork optimization based DTC for enhanced performance of IM based electric vehicle

Anjan Kumar SAHOO[1,*], **Ranjan Kumar JENA**[2]
[1]Department of Electrical Engineering, Biju Patnaik University of Technology, Rourkela, India
[2]Department of Electrical Engineering, Centre for Advanced Post Graduate Studies,
Biju Patnaik University of Technology, Rourkela, India

Received: 17.05.2022 • **Accepted/Published Online:** 18.01.2023 • **Final Version:** 23.03.2023

Abstract: The tailpipe emissions caused by vehicles using internal combustion engines are a significant source of air pollution. To reduce the health hazards caused by air pollution, advanced countries are now adopting the use of electric vehicles (EVs). Due to the advancement of electric vehicles, research and development efforts are being made to improve the performance of EV motors. With a nominal reference stator flux, the classical induction motor drive generates significant flux, torque ripple, and current harmonics. In this work, a teamwork optimization algorithm (TOA)-based optimal stator flux strategy is suggested for torque ripple reduction applied in a classical direct torque-controlled induction motor drive. The suggested algorithm's responsiveness is investigated under various steady-state and dynamic operating conditions. The proposed DTC-IM drive's simulation results are compared to those of the classical and fuzzy DTC-IM drives. The proposed system has been evaluated and found to reduce torque ripple, flux ripple, current harmonics, and total energy consumption by the motor. Further, a comparative simulation study of the above methods at different standard drive cycles is presented. Experimental verification of the proposed algorithm using OPAL-RT is presented. The results represent the superiority of the proposed algorithm compared to the classical DTC and fuzzy DTC IM drives. The torque ripple reduction approach described in this study can also be applied to all induction motors, not only those for electric vehicles or hybrid electric vehicles (HEVs).

Key words: Torque ripple, induction motor, electric vehicle, direct torque control, teamwork optimization, THD

1. Introduction

The global climate and environment are under severe threat as a result of carbon emissions from internal combustion engine-powered cars. The growing usage of fossil fuel vehicles is a significant contributor to global warming and climate change concerns [1]. According to a recent study, transportation accounts for 24% of worldwide carbon dioxide emissions. Another research conducted by the European Union indicates that the transport industry accounts for around 27% of carbon dioxide (CO_2) emissions, with road transport accounting for 70% of emissions directly [2]. To address these issues, electric vehicles have garnered widespread interest worldwide because of their zero greenhouse gas emissions, minimal noise, lightweight construction, enhanced performance, and great efficiency [3].

The electrical motor drive is the critical enabler technology for electric and hybrid vehicles. Permanent magnet synchronous motors (PMSM) and induction motors (IMs) are the most widely accepted motors for vehicle applications due to their high energy and torque densities, higher efficiency, and many other advantages,

*Correspondence: anjank.sahoo@gmail.com

as presented in [4]. An induction motor is regarded as the best choice for electric vehicle application in the metropolitan driving cycle due to its low cost, less maintenance, good efficiency, and reliability [5]. Induction motor drive control techniques are well-documented in the literature. To achieve fast dynamic response, direct torque control (DTC) and field-oriented control (FOC) are frequently utilized in IM drives. Because of its simplicity, DTC looks to be highly useful for EV applications. It does not require any speed or position encoders and only estimates the flux and torque using the observed voltage and current [4]. It also features a quicker dynamic torque response, a low switching frequency, no current regulator, coordinates transformation, and is insensitive to motor parameters other than stator winding resistance. Despite its advantages, traditional DTC has significant downsides, such as high switching loss and torque ripple because of hysteresis bands and the availability of restricted voltage vectors [4].

Several approaches for reducing torque ripple have been documented in the literature [5]. The duty ratio control technique [6] is one of them. The minimum torque-ripple condition determines the pulse duration of the output voltage vector in duty ratio control. Though this substantially improves torque ripple, it enhances the intricacy of the DTC algorithm, and the selection of duty ratio is also critical. The space vector modulation (SVM) approach [7] is another way of reducing ripples. A preview approach is utilized at each cycle to acquire the voltage space vector necessary to precisely adjust for the flux and torque errors. DTC-SVM eliminates the need for hysteresis controllers and switching tables found in conventional DTC systems. However, it necessitates the online computation of multiple complex equations and is dependent on other machine parameters. While the DTC-SVM technique achieves superior performance with a simpler algorithm complexity, it comes at the cost of increased computation time as compared to conventional DTC [8].

The authors in [9] employ fuzzy logic control (FLC) to enhance the performance of the DTC-IM drive. The fundamental benefit of FLC is that it estimates stator resistance change and reduces the developed torque ripple, resulting in accurate and faster operation, as well as dynamic and robust performance. Due to this superiority, it is heavily emphasized in industrial applications [10]. A novel fuzzy adaptive speed regulator with a weighting factor tuning technique was proposed to reduce flux and torque ripple produced by inaccuracies in external sensors and an unsuitable weighting factor over a wide speed range [11]. In [12], a modified brain emotional controller (MBEC) technique for minimizing torque and flux ripples in sensorless induction motor drives is proposed. A biologically inspired intelligent speed controller is used to enhance the system's performance. The speed error is determined by integrating MRAS with SVM to operate sensorless DTC. With the integration of the sensory cortex into the BEC and the accumulation of other limbic system components, the response becomes fast.

The stator flux reference magnitude has a considerable effect on the torque ripples in DTC. The nominal stator flux value is not appropriate for a wide range of load profiles. As a result, the reference flux is optimized in response to the torque to limit torque ripple [13]. In [14], fuzzy logic is used as a stator flux optimizer to select the reference flux value in DTC. The fuzzy membership functions, on the other hand, are asymmetric over the operational range. Adaptive neuro-fuzzy inference systems, artificial neural networks (ANN), and fuzzy logic are used to optimize the reference flux via torque variations [15]. These soft computing approaches are not widely used in electric vehicle applications due to the high computational costs and complexity of the system.

In this paper, a novel torque ripple controller based on optimized stator flux selection is proposed. The TOA is used to estimate the optimized value of the stator reference flux corresponding to the instantaneous speed and torque magnitude. This technique aims to improve torque ripple under both steady-state and dynamic operating conditions. The usefulness of the suggested method is demonstrated, and the motor's speed response

and torque ripple are studied for various vehicle operating modes using simulation and experimental data. The dynamics of the proposed methodology are compared with classical DTC and fuzzy DTC and presented in this paper through a simulation study. A comprehensive analysis with different standard drive cycles is also presented. The results presented in the paper also represent a reduction in flux ripple, current harmonics, and energy consumption, along with the reduction in torque ripple.

2. Conventional direct torque control

The authors in [16, 17] discuss the conventional DTC for IM. DTC has the objective of controlling the machine's electromagnetic torque and flux in a decoupled manner. The dynamic characteristics and control algorithm of the induction motor are described here with the help of the following equations as described by [18].

$$\begin{cases} \overline{V}_s = R_s \overline{I}_s + \frac{d\overline{\psi}_s}{dt} \\ 0 = R_r \overline{I}_r + \frac{d\overline{\psi}_r}{dt} - j\omega\overline{\psi}_r \end{cases} \tag{1}$$

$$\begin{cases} \overline{\psi}_s = L_s \overline{I}_s + L_M \overline{I}_r \\ \overline{\psi}_r = L_r \overline{I}_r + L_M \overline{I}_s \end{cases} \tag{2}$$

The machine equations can be represented in the state variable form considering stator and rotor fluxes are used as state variables as per Equation 3:

$$\frac{d}{dt}\begin{bmatrix} \overline{\psi}_s \\ \overline{\psi}_r \end{bmatrix} = \begin{bmatrix} \frac{-R_s}{\sigma L_s} & \frac{R_s L_m}{\sigma L_s L_r} \\ \frac{R_r L_m}{\sigma L_s L_r} & j\omega - \frac{R_r}{\sigma L_s L_r} \end{bmatrix} \begin{bmatrix} \overline{\psi}_s \\ \overline{\psi}_r \end{bmatrix} + \begin{bmatrix} 1 \\ 0 \end{bmatrix} \overline{v}_s \ , \tag{3}$$

where R_s, and R_r are the stator and rotor resistances. L_s, L_r and L_m are self-inductance of the stator, rotor, and mutual inductance between them. ψ_s, and ψ_r are stator and rotor flux vectors, respectively. ω is the angular rotor speed measured in electrical radian.

The electromagnetic torque equations expressed as a function of state variables are given by [19]:

$$\begin{cases} T_{em} = \frac{3pL_m}{2\sigma L_s L_r} Im\left\{\psi_s . \psi_r{}^*\right\} \\ J.\frac{d\Omega}{dt} + f.\Omega = T_{em} - T_r \ . \end{cases} \tag{4}$$

Using Equation 3, the stator flux can be calculated as shown in Equations 5 and 6 [16] in the stationary reference frame:

$$\overline{\psi}_s(t) = \int_0^t \left(\overline{V}_s(t) - R_s \overline{i}_s(t)\right) dt \ . \tag{5}$$

From Equation 3, the stator flux components along the d and q axis are given as

$$\begin{cases} \psi_{ds}(t) = \int \left(V_{ds}(t) - R_s i_{ds}(t)\right) dt \\ \psi_{qs}(t) = \int \left(V_{qs}(t) - R_s i_{qs}(t)\right) dt \ . \end{cases} \tag{6}$$

Using Equation 6, the magnitude and phase angle of the stator flux in the stationary reference frame can then be estimated as

$$\psi_s = \sqrt{\psi_{ds}^2 + \psi_{qs}^2} \qquad and \qquad \theta_s = \tan^{-1}\frac{\psi_{qs}}{\psi_{ds}} \ . \tag{7}$$

In DTC from the measured voltages and currents in *abc* frame can be transferred to its corresponding values in *dq* reference frame by using Clarke transformation using Equation 8.

$$\begin{bmatrix} v_{qs} \\ v_{ds} \\ v_{0s} \end{bmatrix} = \frac{2}{3} \begin{bmatrix} \cos\theta & \cos(\theta-120) & \cos(\theta+120) \\ \sin\theta & \sin(\theta-120) & \sin(\theta+120) \\ 0.5 & 0.5 & 0.5 \end{bmatrix} \begin{bmatrix} v_{as} \\ v_{bs} \\ v_{cs} \end{bmatrix} \tag{8}$$

As per Equation 6, the stator resistance (R_s) must be known to estimate electromagnetic torque and stator flux. However, for simplicity neglecting resistance, we can have [17]

$$\Delta\overline{\psi}_s = \overline{V}_s \Delta t \ . \tag{9}$$

As per Equation 9 the application of a stator voltage vector for a small period of time can regulate the stator flux. Hysteresis controllers are used to control the magnitude of the flux by selecting appropriate increments in the voltage vector to keep the flux within the prescribed hysteresis band. A two-level hysteresis comparator is used to regulate the stator flux, while a three-level hysteresis comparator is used to control the electromagnetic torque [17]. The outputs are estimated by the electromagnetic torque and stator flux errors, which are called δT_e and $\Delta\Psi_s$, respectively, as indicated in Equations 10 and 11. The corresponding hysteresis bandwidths are represented by HBT_e and HB_Ψ, respectively.

$$HT_e = \begin{cases} 1 & for\ \Delta T_e > HBT_e \\ 0 & for\ -HBT_e < \Delta T_e < HBT_e \\ -1 & for\ \Delta T_e < -HBT_e \end{cases} \tag{10}$$

$$H_\psi = \begin{cases} 1 & for\, \Delta\psi_s > HB_\psi \\ -1 & for\, \Delta\psi_s < -HB_\psi \end{cases} \tag{11}$$

The stator flux reference, as expressed in Equation 12, may be computed using the motor's specifications to ensure that it is sufficient to provide the reference torque.

$$|\psi_s^*| = \sqrt{\frac{4L_s^2 L_r}{3pL_m^2}} \tag{12}$$

2.1. PI speed controller

This has been frequently utilised in conventional DTC due to its simplicity and ability to deliver adequate performance across a broad range of speed operation [20]. It also reduces steady-state inaccuracy and enhances the system's dynamic performance. Therefore, the bulk of published speed control systems for induction motor drives use a basic PI controller with a fixed gain to acquire the reference torque. On the basis of Equation 13, the reference speed is compared to the actual speed, and the error speed is input into the constant gain PI speed controller to generate a reference torque command. The control signal of the PI controller in this study is the torque reference signal, which can be obtained with the expression:

$$\begin{cases} E\Omega_r = \Omega_r^* - \Omega_r \\ T_e^* = K_p E\Omega_r + K_i \int E\Omega_r dt \ . \end{cases} \tag{13}$$

3. Proposed torque ripple reduction algorithm in DTC

In conventional DTC, owing to the inclusion of hysteresis-band, the switching frequency is variable, which generates current distortion and torque ripples. The purpose of the section is to develop the expression of torque ripple and to evaluate the expression of optimum stator flux to reduce the torque ripple.

3.1. Expression of torque ripple

For a small span of time Δt, the stator and rotor fluxes at time may be computed using Equation 3 as follows:

$$\begin{cases} \overline{\psi}_{s_{K+1}} = \overline{\psi}_{s_K} + \frac{d\overline{\psi}_{s_K}}{dt}\Delta t \\ \overline{\psi}_{r_{K+1}} = \overline{\psi}_{r_K} + \frac{d\overline{\psi}_{r_K}}{dt}\Delta t \ . \end{cases} \tag{14}$$

Substituting Equation 3 in 14, it can be rewritten as

$$\begin{cases} \overline{\psi}_{s_{K+1}} = \overline{\psi}_{s_K} + \left(-R_s\frac{\Delta t}{\sigma L_s}\overline{\psi}_{s_K} + \frac{R_s L_m}{\sigma L_s L_r}\overline{\psi}_{r_K} + V_{s_K}\right)\Delta t \\ \overline{\psi}_{r_{K+1}} = \overline{\psi}_{r_K} + \left(\frac{R_r L_m}{\sigma L_s L_r}\overline{\psi}_{s_K} + \left(j\omega_K - \frac{R_r}{\sigma L_r}\right)\overline{\psi}_{r_K}\right)\Delta t \ . \end{cases} \tag{15}$$

Equation 15 expresses the flux of the induction machine in discrete form, valid for a small finite interval Δt. It is worth noting that in Equation 15, the change in stator flux is due to the applied stator voltage vector for a specific operating state, even though the applied voltage vector is not explicitly mentioned. The stator flux variation is used to illustrate the influence on the rotor flux.
From Equation 4, the developed motor torque in the $(K+1)^{th}$ instance can be written as

$$T_{K+1} = \frac{3pL_m}{2\sigma L_s L_r} Im\left\{\overline{\psi}_{s_{K+1}}.\overline{\psi}^*_{r_{K+1}}\right\} \ . \tag{16}$$

Substituting Equation 15 in 16 and excluding higher-order Δt terms for simplicity, the torque at $(K+1)^{th}$ instance can be expressed as

$$T_{K+1} = T_K - T_K\left(\frac{R_s}{L_s} + \frac{R_r}{L_r}\right)\frac{\Delta t}{\sigma} + \frac{3pL_m}{2\sigma L_s L_r}.\Delta t.Im\left\{\overline{V}_{s_K}\overline{\psi}^*_{r_K} - j\omega_K\left[\overline{\psi}_{s_K}.\overline{\psi}^*_{r_K}\right]\right\} \ . \tag{17}$$

Equation 17 may be rewritten as

$$\Delta T = T_{K+1} - T_K = \Delta T_{K1} + \Delta T_{K2} \ , \tag{18}$$

where $\Delta T_{K1} = -T_K\left(\frac{R_s}{L_s} + \frac{R_r}{L_r}\right)\frac{\Delta t}{\sigma}$, and $\Delta T_{K2} = \frac{3pL_m}{2\sigma L_s L_r}.\Delta t.Im\left\{\overline{V}_{s_K}\overline{\psi}^*_{r_K} - j\omega_K\left[\overline{\psi}_{s_K}.\overline{\psi}^*_{r_K}\right]\right\}$.
The first component is caused by the machine parameters and tends to diminish the torque magnitude. This is independent of the stator voltage and rotor speed in the instantaneous state but depends on the instantaneous torque magnitude. The second component denotes the influence of the applied voltage vector on the variation of torque and is dependent on system parameters such as rotor speed and torque. Equation 18 can be further expanded and simplified as

$$\Delta T = -K\,T_K\Delta t + \frac{3pL_m}{2\sigma L_s L_r}.\Delta t.Im\left\{\overline{V}_{s_K}\overline{\psi}^*_{r_K} - j\omega_K\left[\overline{\psi}_{s_K}.\overline{\psi}^*_{r_K}\right]\right\} \ , \tag{19}$$

where $K = \frac{1}{\sigma}\left(\frac{R_s}{L_s} + \frac{R_r}{L_r}\right)$.

After further simplification, the torque ripple expression can be written as

$$\Delta T = \frac{3pL_m}{2\sigma L_s L_r}\Delta t.Im\left\{\overline{V}_{s_K}\overline{\psi}^*_{r_K} - (K + j\omega_K)\left(\overline{\psi}_{s_K}.\overline{\psi}^*_{r_K}\right)\right\} . \tag{20}$$

Using Equations 1 and 2, under the steady-state condition, the relation between stator flux and rotor flux can be expressed as

$$\psi_s = \frac{L_s R_r - j\left(L_m^2 - L_s L_r\right)(\omega - \omega_s)}{L_m R_r}\psi_r = (a + jb)\psi_r \ , \tag{21}$$

where $a = \frac{L_s}{L_m}$, and $b = \frac{\left(L_m^2 - L_s L_r\right)(\omega - \omega_s)}{L_m R_r}$.

Using Equation 21 in 20 the torque ripple expression as a function of rotor flux, speed and stator voltage can be formulated as

$$\Delta T = \frac{3pL_m}{2\sigma L_s L_r}.\Delta t.Im\left\{V_s\psi_r^* - (K + j\omega)(a + jb)(\psi_s.\psi_r^*)\right\} . \tag{22}$$

After further simplification and considering only the imaginary part, Equation 22 can be further expanded as

$$\Delta T = \frac{3pL_m}{2\sigma L_s L_r}.\Delta t.\left\{(V_{qs}\psi_{dr} - V_{ds}\psi_{qr}) - (a\omega + bK)\left(\psi_{dr}^2 + \psi_{qr}^2\right)\right\} . \tag{23}$$

If the reference frame is aligned on the rotor flux axis, then the torque ripple in the motor can be calculated as

$$\Delta T = \frac{3pL_m}{2\sigma L_s L_r}.\Delta t\left\{V_{qs}\psi_{dr} - \left(\frac{\omega L_s}{L_m} + \frac{K\left(L_m^2 - L_s L_r\right)(\omega - \omega_s)}{L_m R_r}\right)\psi_{dr}^2\right\} . \tag{24}$$

3.2. TOA-based optimal stator flux selection

Population-based optimization algorithms are popular techniques for tackling optimization issues. In this article, a new population-based stochastic algorithm known as the teamwork optimization algorithm has been considered for selecting the optimal reference flux to reduce the torque ripples. The primary benefit of TOA is that it is a nonparameterized online approach that tends toward optimum efficiency.

The most important thing to remember about any optimization process is that it is impossible to claim that a single method is the best optimizer under all circumstances. All the optimization algorithms have their own limitations. Hence, new optimization algorithms can be developed at any time to generate solutions that are closer to the global optimal solution.

As described in [21], to study the effectiveness of the proposed optimal algorithm, it was compared with eight commonly used optimization algorithms with the help of 23 standard objective functions. The proposed algorithm is able to provide global optimal solutions for eight objective functions. On the other hand, the proposed algorithm involves simple equations that are easy to use, no control parameters, the right amount of exploitation and exploration, does not get stuck in local optimal solutions, and has a strong ability to converge.

3.2.1. Description of TOA

The algorithm's primary objective is to imitate team members' collaborative behaviours to accomplish a goal. TOA is theoretically described to ensure that it can solve optimization issues as presented in [21]. The method is a population-based optimization algorithm built on simulations of team members' interactions and behaviours

while completing their jobs and accomplishing the team's intended objective. Thus, search agents are regarded as team members in TOA, and links between team members serve as a mechanism for the transfer of information.

In TOA, every member of the population comes up with an idea for how to solve the optimization problem. In reality, each person in the population gives a value for the variable that is being looked at. This means that each person in the population can be shown mathematically as a vector with as many parts as there are variables in the problem. The values for the objective function are derived by putting the proposed values by the teammates into the objective function's variables. Therefore, a value for the objective function is determined for each member of the population. In each iteration of the algorithm, the team member with the best performance is picked as the supervisor by comparing the objective function's values. In teamwork, the supervisor is responsible for leading the team and guiding the team members to reach the team's objective.
TOA updates the algorithm population in three steps.
Stage 1: Supervisor guidance
This stage involves updating team members as per the instructions of the supervisor. At this point, the supervisor communicates with the members and steers them toward the goal. Equation 25 is used to model this update stage in TOA.

$$\begin{cases} X_i^{S1} : x_{i,d}^{S1} = x_{i,d} + r\left(s_d - I \times x_{i,d}\right), \\ X_i = \begin{cases} X_i^{S1}, F_i^{S1} < F_i \\ X_i, \quad else \end{cases} \\ I = round(1 + r)\ , \end{cases} \tag{25}$$

where ${F_i}^{s1}$ is the value of the objective function, ${X_i}^{s1}$ represents the updated weight of d^{th} problem variable as recommended by an i^{th} team member following supervisor guidance, r is a random number between [0, 1], and I is the updation-index.
Stage 2: Information sharing
Here, each member of the team competes to enhance their performance by utilizing the information from other teammates who have performed better than them. The team members of the proposed TOA are updated based on Equations 26 and 27.

$$X^{M,i} : x_d^{M,i} = \frac{\sum_{j=1}^{N_i} x_{j,d}^{g,i}}{N_i}, \tag{26}$$

$$\begin{cases} X_i^{S2} : x_{i,d}^{S2} = x_{i,d} + r\left(x_d^{M,i} - I \times x_{i,d}\right) \times sign\left(F_i - F^{M,i}\right), \\ X_i = \begin{cases} X_i^{S2}, F_i^{S2} < F_i \\ X_i, \quad else\ , \end{cases} \end{cases} \tag{27}$$

where $F^{M,i}$ and ${F_i}^{s2}$ are the values of the objective functions, $X^{M,i}$ is the team's average having higher than that of the i^{th} team member, N_i is the number of members who outperform compared to an i^{th} teammate, $x_{j,d}^{g,i}$ is the value of the d^{th} variable recommended by the j^{th} better team member for the i^{th} teammate, ${X_i}^{s2}$ is the second stage updated status of an i^{th} teammate.
Stage 3: Individual activity
Each member endeavours to enhance their performance based on the present position in this stage. Equation 28 represents the updation of teammates for this stage.

$$\begin{cases} X_i^{S3} : x_{i,d}^{S3} = x_{i,d} + (-0.01 + 0.02r)\, x_{i,d} \\ X_i = \begin{cases} X_i^{S3}, F_i^{S3} < F_i \\ X_i, \quad else\ , \end{cases} \end{cases} \tag{28}$$

where F_i^{s3} is the value of the objective function and X_i^{s3} is the final status of an i_{th} team member. The population is updated in three stages for each iteration of the algorithm according to Equations 25–28. The iterative process is repeated until the algorithm reaches the stop criteria. Finally, TOA provides the optimal solution to the optimization problem.

3.2.2. Implementation of TOA for optimal flux selection

In this work, TOA is used to calculate the optimum stator flux for minimizing the torque ripple while satisfying the system constraints. Figure 1 depicts the architecture of the DTC-based IM drive for EV with the recommended loss minimization technique.

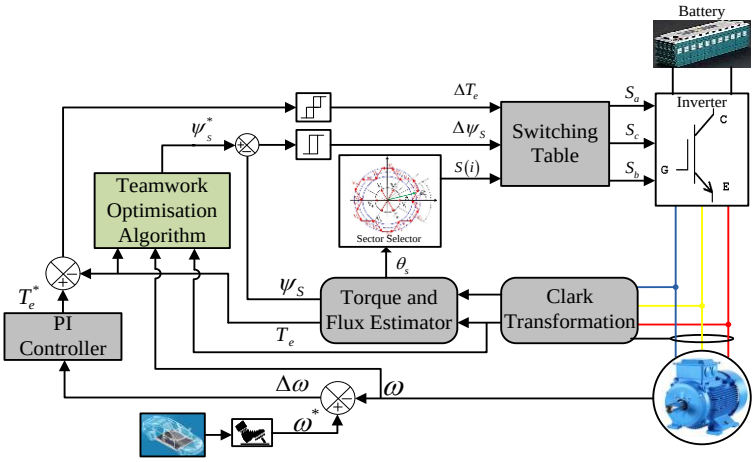

Figure 1. Block diagram of the proposed DTC for EVs.

1. *Objective function*
   From an induction motor point of view, torque ripple reduction is the prime objective for selecting the reference stator flux. The torque ripple of the induction motor can be expressed as formulated in Equation 28. Therefore, the objective function can now be formulated using Equation 28

$$f = min(T_{ripple}) \ . \tag{29}$$

2. *Constraints*
   The objective function described in Equation 29 is optimized using TOA for the following pragmatic constraints.

   - d-axis rotor flux: The d-axis rotor flux is allowed to vary within the minimum and maximum permissible rotor flux.

$$\psi_{dr}^{min} \leq \psi_{dr} \leq \psi_{dr}^{max} \ , \tag{30}$$

   where $\psi_{dr}^{min} = 0.2$Wb and $\psi_{dr}^{max} = 1.1$Wb.

3. *Generation of the initial population*
   In the present work, TOA is used to compute the optimal d-axis rotor flux, to minimize the power loss of

the induction machine. The initial population of the TOA contains the uniformly distributed d-axis rotor flux values as specified by Equation 31.

$$X_i = \psi_{dr}^{min} + rand \times \left(\psi_{dr}^{max} - \psi_{dr}^{min}\right) \tag{31}$$

For example the first population may be calculated as $X_1 = 0.2 + rand \times (1.1 - 0.2) : X_1 = 0.3457$.

4. *Detail steps of implementation*
The following flow chart describes the detailed implementation steps of the proposed algorithm to minimize the power loss of the induction machine is described in the flow chart as shown in Figure 2.

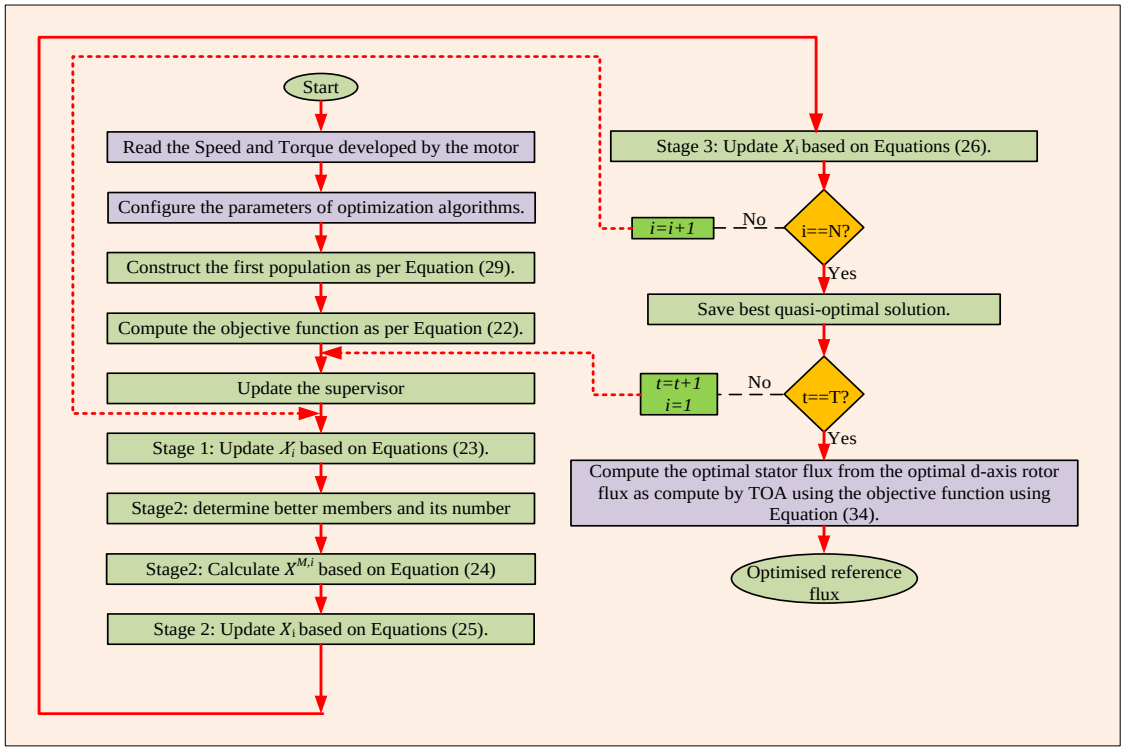

Figure 2. Flowchart of the proposed TOA.

However, as stator flux control is required for a DTC-based IM drive, a simple conversion between stator and rotor fluxes may be employed. As a consequence, the optimal reference value for stator flux is as follows:

$$\psi_s^* = \psi_s^{ref} = \frac{L_s}{L_m}\sqrt{(\psi_{dr}^*)^2 + \left(\frac{2}{3}\frac{\sigma L_r}{p}\right)^2 \left(\frac{T_e^{ref}}{\psi_{dr}^*}\right)^2} \ . \tag{32}$$

4. Results and discussion

To evaluate the effectiveness of the suggested TOA-based stator flux and the proposed optimized DTC, a simulation-based comparison among conventional DTC [17], and Fuzzy DTC [9], and proposed DTC is presented here. Table 1 depicts the specifications of the induction motor utilized in the simulation study. The simulations are conducted in MATLAB/Simulink environment with a simulation step time (sampling time) of $25\,\mu s$.

Simulation studies are conducted for all three methodologies under consideration. A speed profile with starting, constant speed, acceleration, and breaking, a profile comparable to that used in electric vehicle applications, is applied, as shown in Figure 3.

Table 1. IM parameter.

Power:	$50HP(37kW)$	$L_s = L_r^{'}$:	0.724e-3H
Voltage:	400V	L_m:	27.11e-3H
R_s:	$82.33e-3\Omega$	Frequency (f):	50Hz
$R_r^{'}$:	$50.3e-3\Omega$	Pole Pair (p):	2

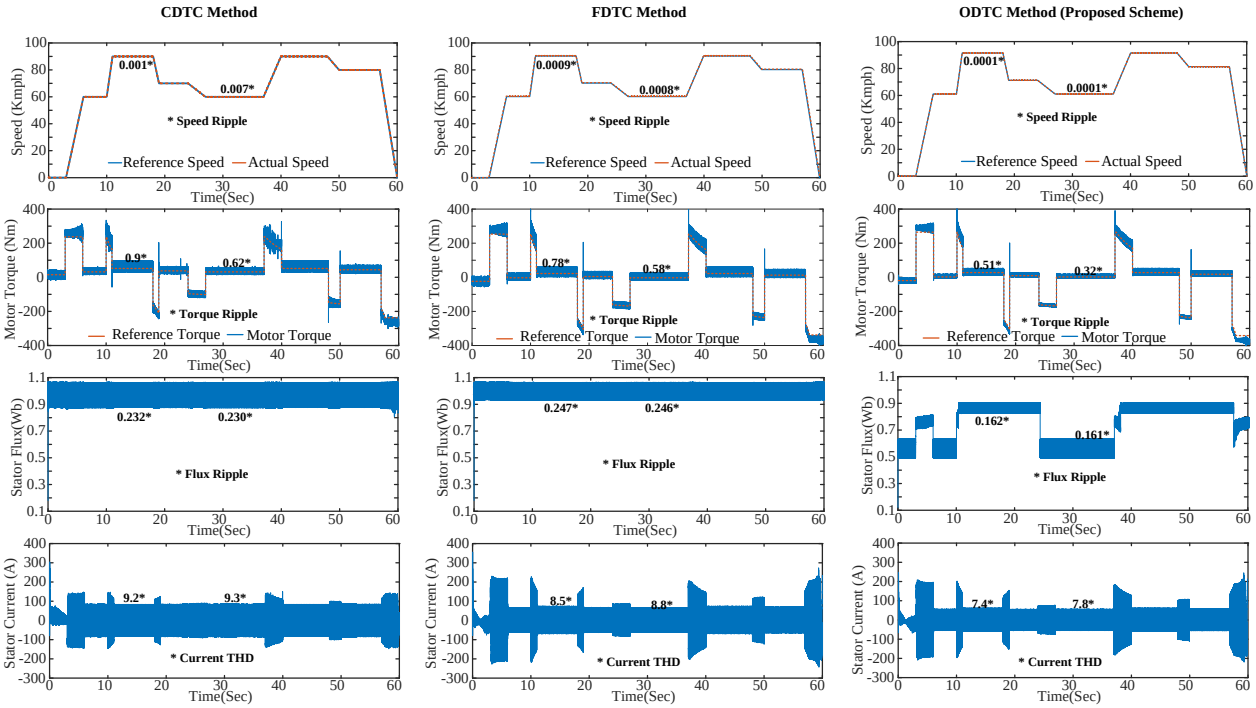

Figure 3. Performance of the electric vehicle with (a) conventional DTC, (b) fuzzy DTC, and (c) optimized DTC methods.

Along with the speed response, Figure 3 depicts the IM's torque, stator flux, and stator current response. The battery current profile and d-axis q-axis stator flux profiles have also been depicted in this figure. As can be seen, the motor's torque response closely matches the reference value; however, the resulting motor torque in optimized DTC has the lowest torque ripple of all. There is a reduction of 38.89% torque ripple in optimized DTC compared to conventional DTC, whereas this is 34.48% with fuzzy DTC. Similarly, the reduction in stator current THD is 17.39% and 10.58% when compared with conventional DTC and fuzzy DTC, respectively. This reduction in torque ripple and THD is due to the optimal selection of stator flux, which can be observed in Figure 3. For conventional DTC and fuzzy DTC, the reference flux is constant as decided from Equation 12; however, the reference flux in optimized DTC is a variable one with speed and load as per Equation 32. Figure 3 also represents the battery current profile, which shows a rise in current drawn with load and charging of the battery during braking due to regenerative power.

To further demonstrate the substantial reduction in the flux, Figure 4 shows the d-q trajectory obtained in the stationary reference frame using the three DTC approaches for the driving cycle as shown in Figure 3. As presented in Figures 4a and 4b, the circular trajectory of the stator flux in a DTC drive. Both the figures indicate a fixed flux magnitude irrespective of the driving scenario and reduced flux ripples in fuzzy based DTC. However, Figure 4c demonstrates a dynamic flux magnitude that corresponds to the operating condition, validating the suggested technique. As proposed in Section 3, it can be observed that the reference flux magnitude varies according to the load profile and at the same time maintains a circular trajectory.

Figure 5 compares the speed error and battery energy for the three controllers. It can be observed that the speed error is the lowest among all DTCs. Table 2 represents the mean square error (MSE) of the speed for the drive cycle as presented in Figure 3. The results indicate the proposed method has the least MSE among all, which indicates a better speed response by the proposed method.

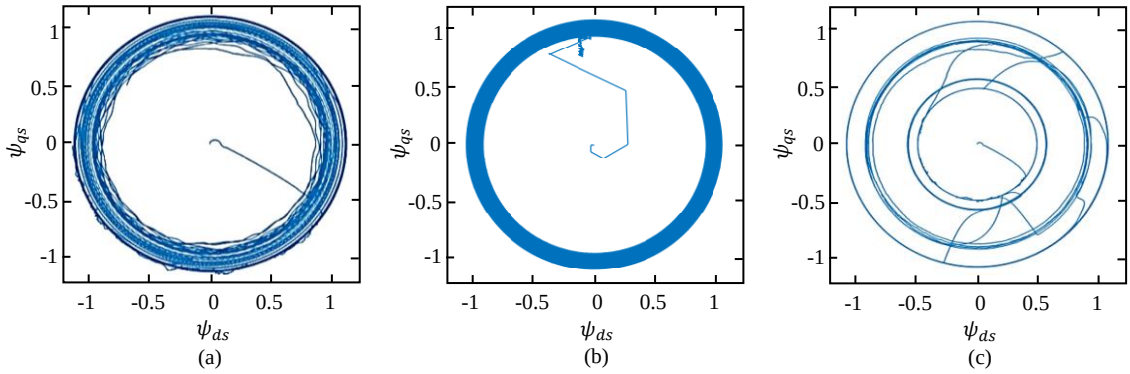

Figure 4. Flux trajectory for (a) conventional DTC, (b) fuzzy DTC, and (c) optimized DTC methods.

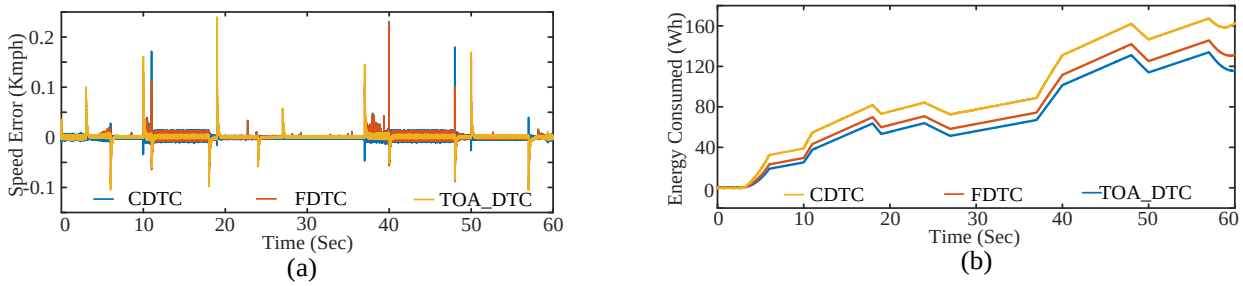

Figure 5. Comparison of (a) speed error and (b) battery energy.

Table 2. MSE of speed error for the drive cycle in Figure 3.

	DTC	Fuzzy DTC	Proposed Method
MSE	9.16e-05	8.2427e-05	6.4595e-05

One of the objectives of this work is to reduce the battery energy consumption by the motor to enhance the driving range in a single charge. To study the energy consumption by different methods, the battery energy consumed during the drive cycle by each method is shown in Figure 5b. Due to the reduction in torque ripple and current THD, the battery energy required to drive the vehicle over the entire cycle is also minimal. It is

found that there is a reduction of 36.2% and 11.8% of total battery energy in optimized DTC compared to conventional DTC and fuzzy DTC, respectively.

4.1. Steady-state performance

To demonstrate the proposed optimized DTC's improved steady-state performance, a complete comparison of conventional DTC, fuzzy DTC, and optimized DTC is undertaken under various operating situations, evaluating flux ripple, torque ripple, and current THD.

Figure 6 plots the low-speed operation results of conventional DTC, fuzzy DTC, and optimized DTC at 20 kmph. To provide a clear picture of the performance of the three approaches, the current harmonic spectra are provided together with the torque, flux, and stator current associated with this speed, from which the current THDs of conventional DTC, fuzzy DTC, and optimized DTC are found to be 9.3%, 7.9%, and 7.3%, respectively. As a result, we can infer that optimized DTC has the lowest current total harmonic distortion and the least distorted current waveform at low speeds. It can be noticed that torque ripple is also minimum among all for optimized DTC, which is 59.31% and 49.72% less compared to conventional DTC and fuzzy DTC, respectively.

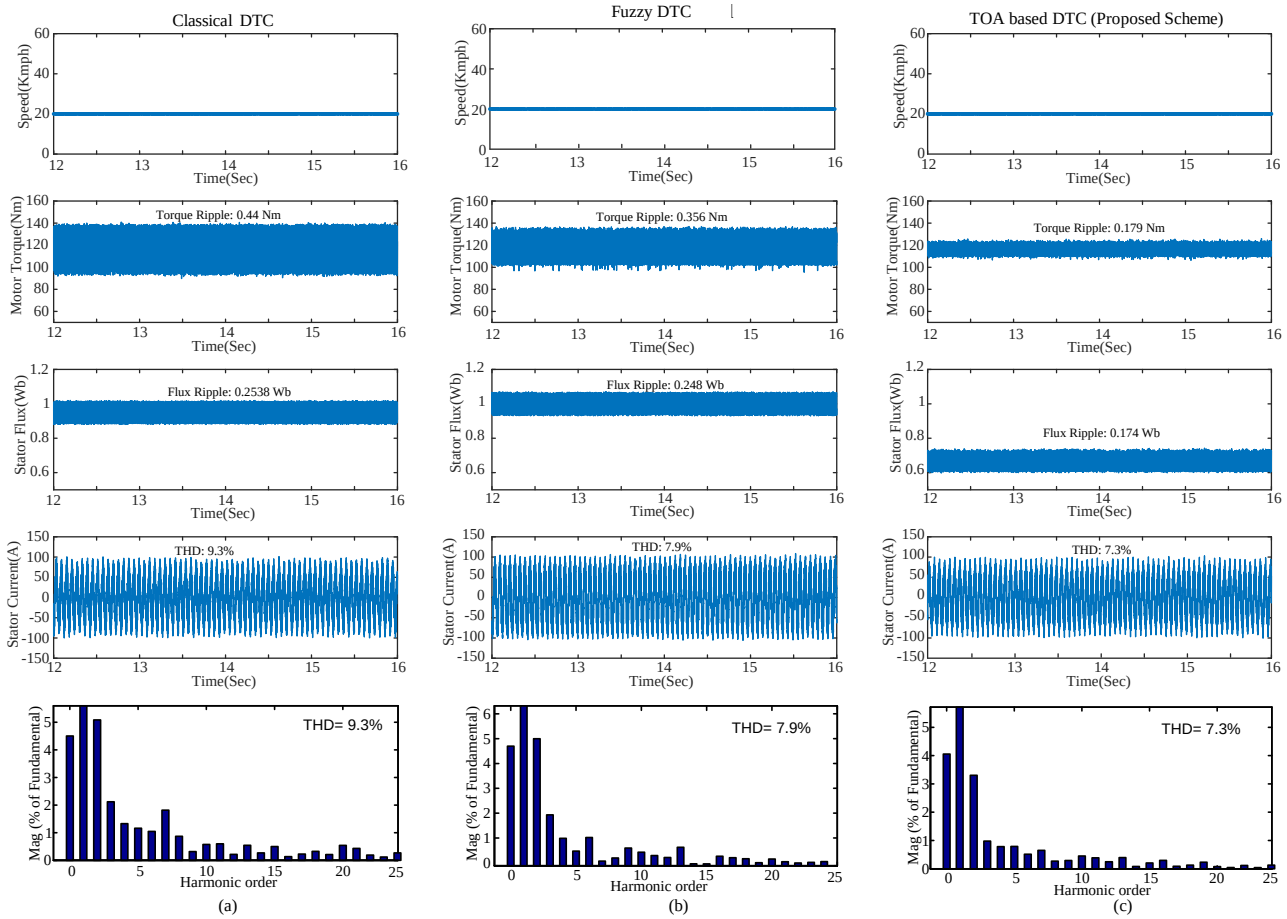

Figure 6. Steady-state performance at low speed for (a) conventional DTC, (b) fuzzy DTC, and (c) optimized DTC methods.

Figure 7 provides the results of conventional DTC, fuzzy DTC, and optimized DTC at a high speed of 80 kmph. The current harmonic spectra are presented, with the current THDs of the three approaches being 9.1%, 7.5%, and 6.5%, respectively. As a result, we may continue to see that optimized DTC has the lowest current THD at high speed as well. Similarly, the torque ripple for the optimized DTC method is minimum for high speed also, which is 28.42% and 20.37% lesser than conventional DTC and fuzzy DTC, respectively. As stated above, the quality of flux and torque control has a direct effect on the current THD of the motor drive. To demonstrate the performance at different operating points, the torque ripple, speed ripple, flux ripple, and stator current THD values of the three approaches were obtained at different speeds and loads and compared in Figure 8.

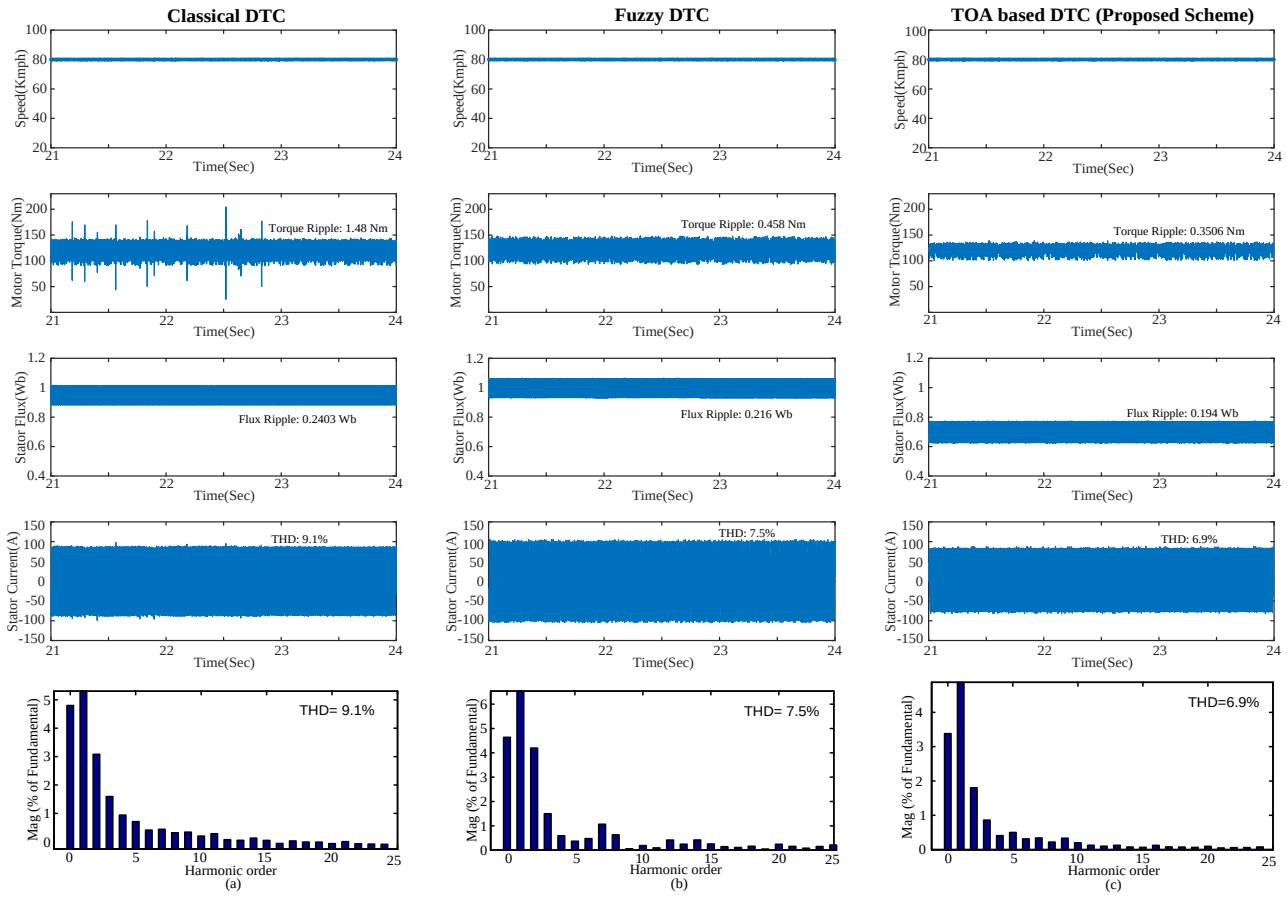

Figure 7. Steady-state performance at high speed for (a) conventional DTC, (b) fuzzy DTC, and (c) optimized DTC methods.

As shown in Figure 8, at 40 kmph, optimized DTC has a lower flux ripple (0.178 Wb) than conventional DTC (0.25 Wb) and fuzzy DTC (0.241 Wb) at all load conditions. Additionally, optimized DTC has the lowest torque ripple of 2.7 Nm, 17.14% less than conventional DTC, and 7% less than fuzzy DTC. Also, the corresponding value of torque ripple in optimized DTC has the minimum value among all methods. With optimized DTC, the stator current THD is significantly reduced compared to the other two for the entire range of load as shown in Figure 8. Analysis at high speed, i.e. at 80 and 100 kmph, demonstrates that the suggested technique outperforms all other methods in terms of torque ripple across all load ranges, though the flux ripples

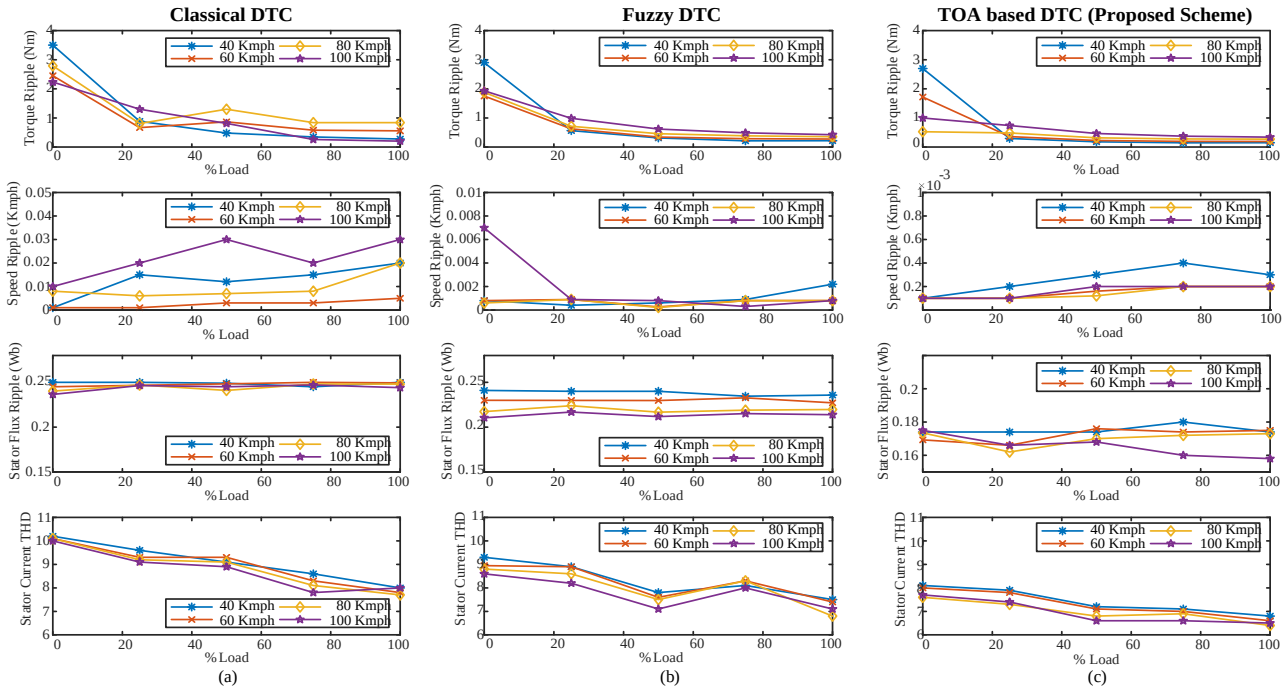

Figure 8. Simulation study: induction motor drive characteristics (electromagnetic torque, speed, stator flux, and stator current THD) under the steady-state condition with (a) conventional DTC, (b) fuzzy DTC, and (c) optimized DTC methods.

of all three approaches are close to each other, with optimized DTC having the minimum value. As a result, it can be concluded that the proposed optimized DTC has superior steady-state performance over conventional DTC and fuzzy DTC in terms of flux and torque ripples, as well as improved harmonics at low and high speeds. Though the speed ripple in all operating conditions with all three methods is very small, there is still some improvement in the speed ripple with the proposed one compared to the other two.

4.2. Dynamic performance

To evaluate the suggested approach's dynamic performance, the results of a simulation study comparing conventional DTC, fuzzy DTC, and optimized DTC with acceleration and braking are depicted in Figures 9 and 10.

The vehicle's starting process may be separated into two stages, preexcitation and acceleration, as seen in Figure 9. The speed reference is 0 kmph during preexcitation, but the flux reference is its nominal value (1 Wb for conventional DTC and fuzzy DTC, whereas only 0.6 Wb for optimized DTC). After the switching transient dies out and the stator flux amplitude arrives at its reference value, the reference speed steadily rises to 60 kmph, indicating that the operation has entered the acceleration phase. Additionally, as seen in Figure 9, the flux magnitude increases to 0.8 Wb as the torque developed by the motor increases during this acceleration process. When the motor accelerates, the real-time torques of conventional DTC, fuzzy DTC, and optimized DTC increase substantially to 150 Nm. Additionally, the time required for the three techniques to achieve the reference speed is almost the same, around 2 ms, indicating that conventional DTC, fuzzy DTC, and optimized DTC all exhibit a comparable dynamic reaction during the acceleration process.

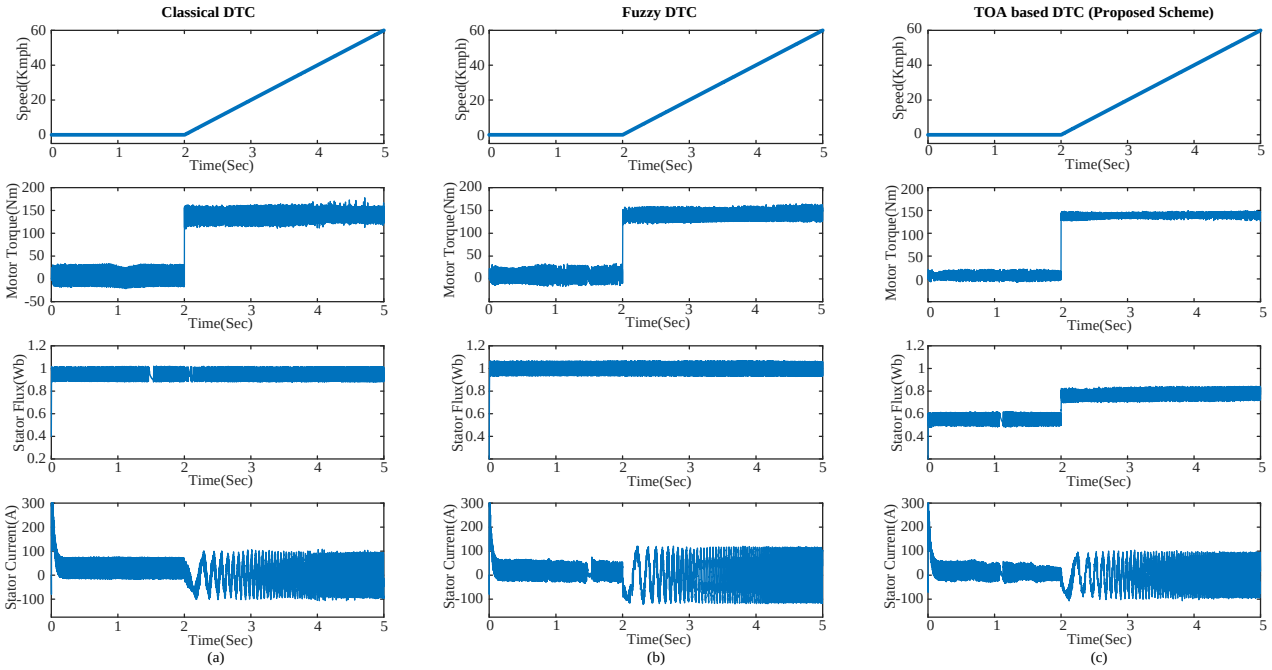

Figure 9. Starting response from zero speed to high speed for (a) conventional DTC, (b) fuzzy DTC, and (c) optimized DTC methods.

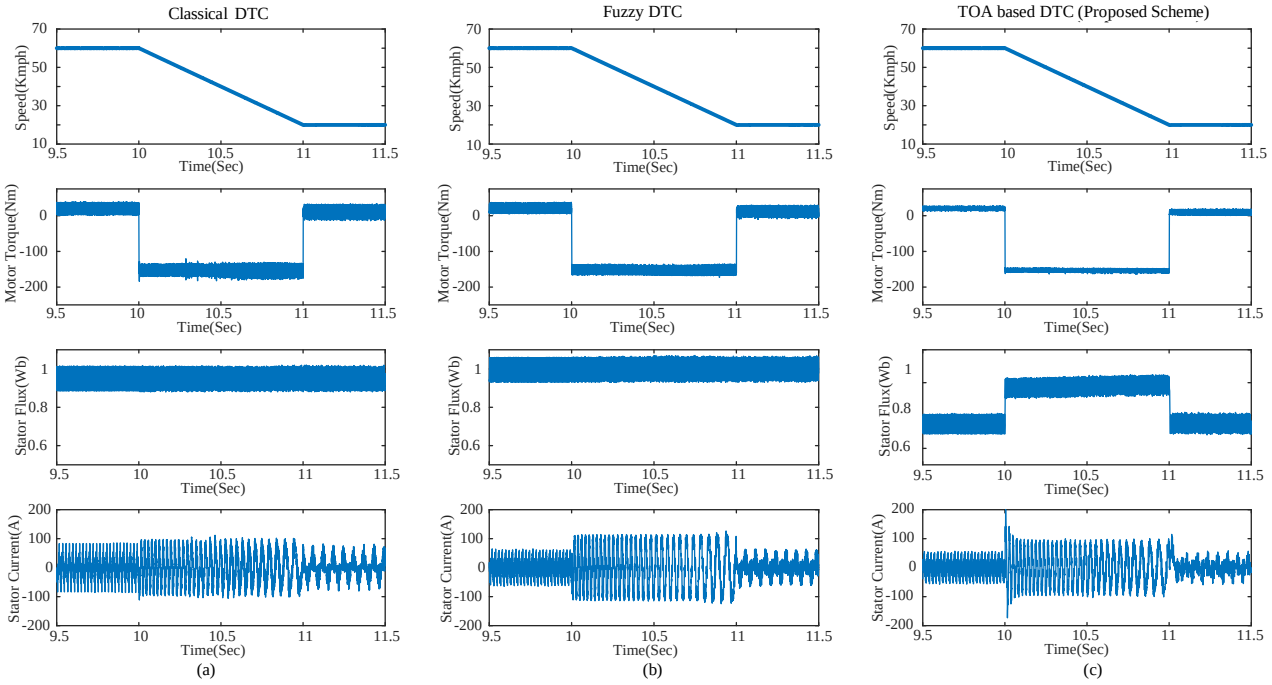

Figure 10. Response during braking for (a) conventional DTC, (b) fuzzy DTC, and (c) optimized DTC methods.

Figure 10 describes the braking of the vehicle with conventional DTC, fuzzy DTC, and optimized DTC. Initially, the speed of the vehicle was 60 kmph; with the application of the brake, it reduced to 20 kmph. All three approaches exhibit a similar speed response, whereas they have different flux and torque responses. For

DTC and fuzzy-based DTC throughout the operation, the reference flux is maintained at a constant magnitude of 1 Wb. However, for the proposed approach, both before and after braking, the reference flux was around 0.75 Wb due to load torque demand and during the transient, the flux level rose to around 0.95 Wb to fulfil the high torque demand. The torque developed by the motor at both steady-state speeds is low, whereas during braking, the motor develops a large negative torque, i.e. around –150 Nm in this case, to bring the speed down more quickly.

4.3. Performance with standard drive cycle

In addition to the above performance, the conventional DTC, fuzzy DTC, and optimized DTC are also tested considering HWFET drive cycles. The simulated results obtained are shown in Figure 11. From the figure, it is clear that the vehicle speed tracks the reference speed, the speed response is similar for all three methods. Similarly, a comparison of response using the ECE R15 drive cycle with DTC and the proposed DTC is presented in Figure 12. In the conventional DTC for both the drive cycles, a significantly large torque ripple is observed; however, this is reduced with fuzzy-based DTC, and with the proposed method, the torque ripple performance is far superior. Similar observations are seen for the flux ripples as well. As the torque and flux ripple of the proposed DTC are less so, the current magnitude is comparatively small compared to the other two. Most importantly, the battery energy consumed by the vehicle in both the drive cycles with optimized DTC is lower as compared to the other two.

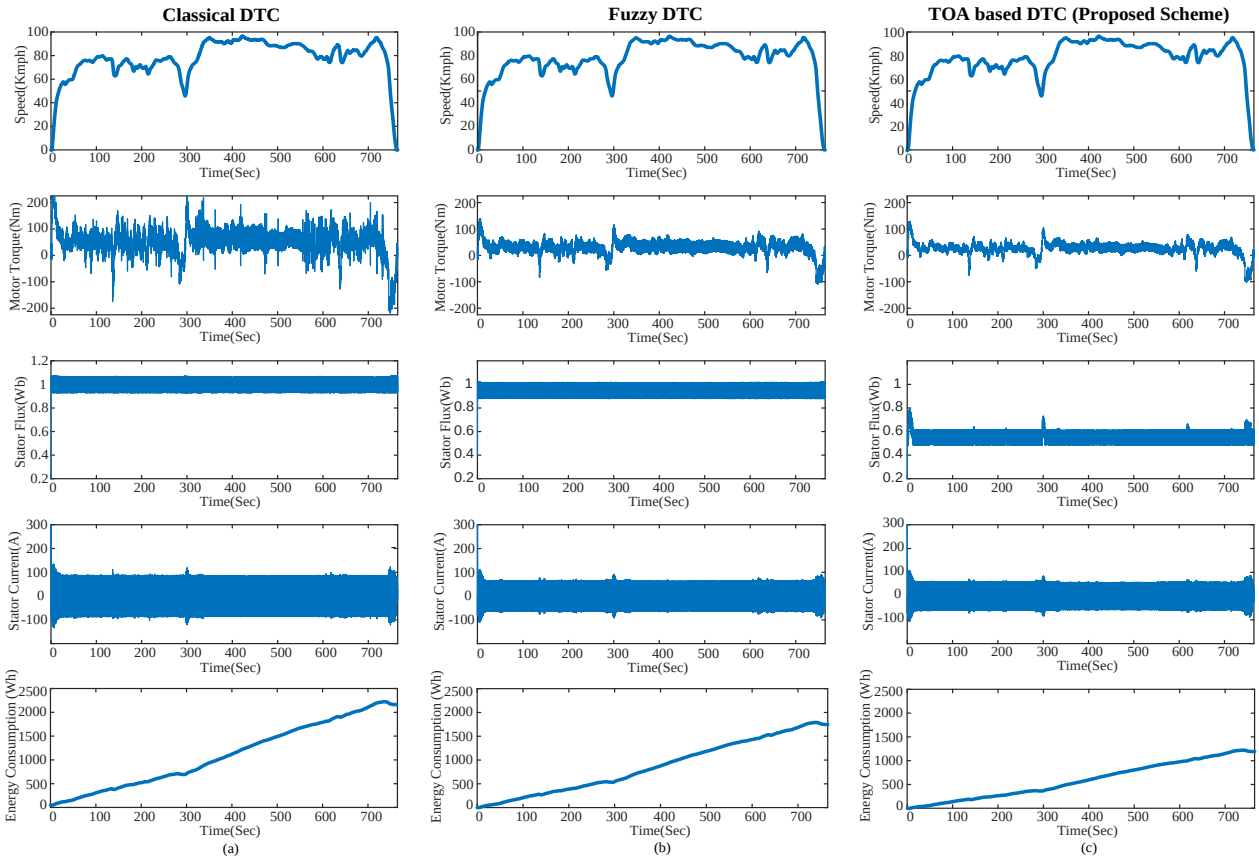

Figure 11. Performance of the electric vehicle under HWFET drive cycle with (a) conventional DTC, (b) fuzzy DTC, and (c) optimized DTC.

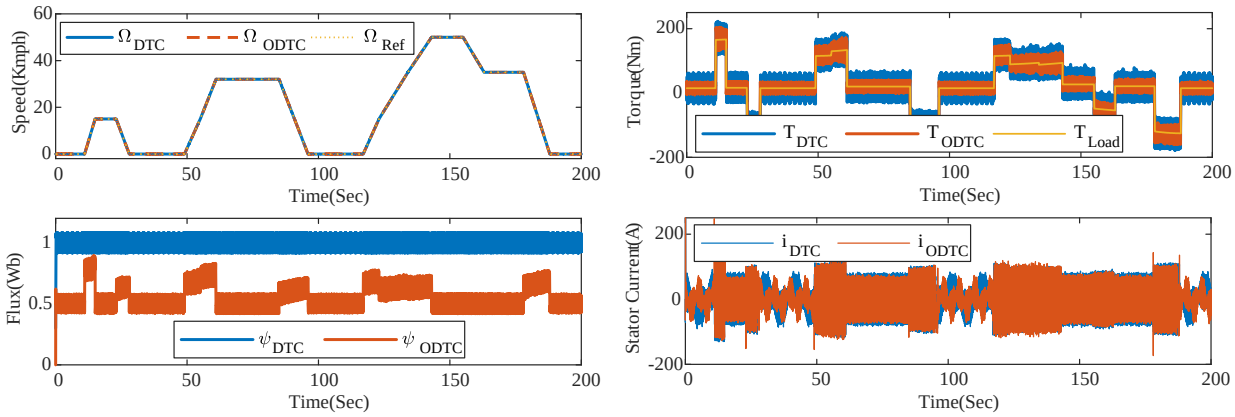

Figure 12. Performance of the electric vehicle under ECE R15 drive cycle.

Table 3. MSE for standard drive cycle.

	Speed		Torque	
	DTC	Proposed DTC	DTC	Proposed DTC
HWFET	2.1604e-5	1.8543e-5	230.701	207.358
ECE R15	1.7534e-5	1.0318e-5	24.5761	20.7758

To analyze the performance of the proposed technique for the standard drive cycle, the mean square error (MSE) of the speed and torque response is calculated and tabulated in Table 3. With the use of optimal flux, the torque ripple reduces, which results in reduced torque error for both drive cycles. A reduction in torque MSE of 10% and 15.46% is observed for the HWFET and ECE R15 drive cycles, respectively.

4.4. Comparison

Table 4 presents a comparison of the proposed method with approaches published in the recent literature. The motor rating can vary depending on the size and weight of the vehicle, and it also differs from the simulated value depending on the actual motor size utilized for testing. For the proposed work, a 37-kW IM traveling at 20 kmph with a load torque of 119 N.m is considered, and an improvement of 59.32% and 49.72%, respectively, is discovered, which is relatively more significant than the other strategies considered.

4.5. Experimental validation using OPAL-RT

The suggested strategy is empirically validated in this study by utilizing an OPAL-RT real-time simulator. The OP4510 OPAL-RT is used in this experiment. The suggested approach is modeled and simulated in software-in-the-loop (SIL) mode utilizing this real-time digital simulator. The fixed time step (sampling time) used in real-time simulation is 25 μs, which is the same as that in simulation.

Figure 13 shows the experimental setup. The performance of the proposed control technique is validated experimentally with the inverter fed 3 HP induction motor, which is mechanically coupled with a DC shunt generator connected to a variable resistive load instead of the speed controller. The dc generator, along with the load box, provides the various load torque to the induction motor. Thus, the DTC approach is maximized by decreasing torque ripple while maintaining torque control capabilities across a wide range of operating speeds.

Table 4. Comparison of IM drive for torque ripple control.

Reference	Methods	Torque ripple (N.m)	Improvement (%)	Operating condition
[12]	SVM DTC MBEC SVM DTC	14.8 7.9	46.62	120 W induction motor driven at the rated condition
[22]	CDTC CSVPWM	6 3.5	41.67	A 5.4 HP motor operated with T_L = 27 Nm.
[23]	CDTC FDTC	25.75 14.7	42.91	A 30 kW motor operated with T_L = 200 Nm.
[24]	HTFC MST-HTFC	0.61 0.28	54.1	1 kW induction motor drive at the rated condition
Proposed work	CDTC FDTC ODTC	0.44 0.356 0.179	59.32 49.72	A 37 kW IM driven at 20 kmph with a load torque of 119 N.m

Figure 13. Experimental setup for the proposed method (A) Host PC, (B) 3-Phase VSI, (C) OpalRt-4510 controller, (D) Induction Motor coupled with DC generator, (E) DSO.

To record the experimental results, a digital storage oscilloscope (DSO) is attached to the simulator's output port and another across the motor.

Figure 14 illustrates the experimental observations and comparison of DTC and the proposed DTC. Both approaches are examined at a speed of 20 kmph and the speed, flux, and responses are compared. The results obtained indicate an improved response and ripple effects with the proposed approach. Figure 14b indicates a

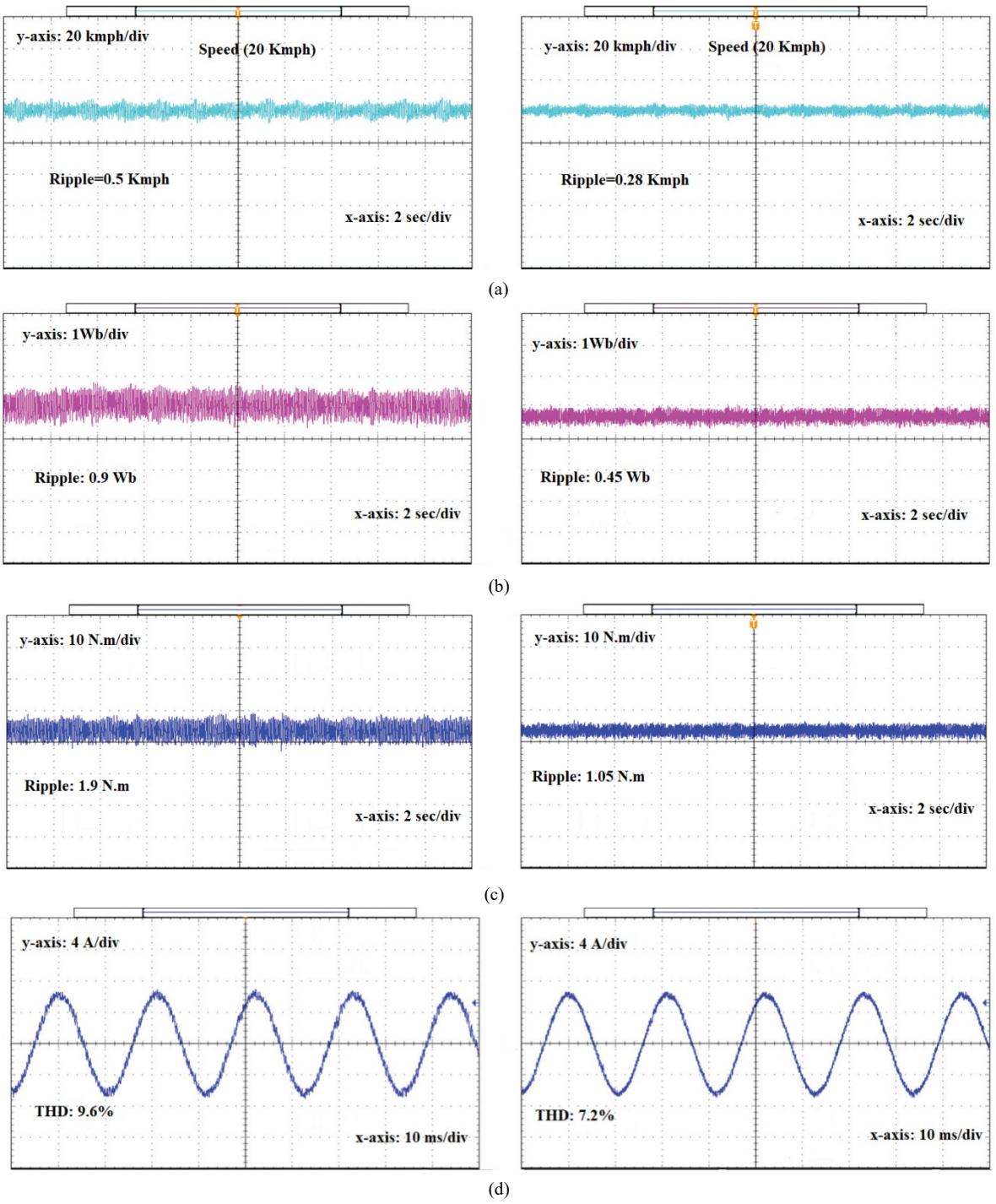

Figure 14. Experimental results at 20 kmph for DTC and the proposed method (a) speed, (b) stator flux, (c) motor torque, (d) stator current.

reduction in flux magnitude and ripples for the same load torque. Fifty percent reduction in flux ripple and 44.7% reduction in torque ripple are estimated with the proposed approach compared to conventional DTC. The response at 20 kmph in the simulation process indicates a reduction of 27% in flux and 59.31% in torque

ripples, so the experimental results exhibit a strong correlation with the simulation results. The observed stator current also show a reduction of 25% THD.

5. Conclusion

A TOA-based reference stator flux selection approach was implemented for an IM drive for electric vehicle applications. The primary purpose of this work was to eliminate torque ripple and stator current harmonics. This is accomplished by introducing the appropriate stator flux based on the instantaneous torque, speed, and voltage. To validate this work, a comprehensive simulation analysis of the suggested algorithm is provided, along with a comparison to conventional DTC and fuzzy DTC over a broad range of speeds and driving scenarios. In the literature, it is found that DTC is mostly used for EV applications, but torque and flux ripples are the major issues with it. Most of the literature used AI-based techniques to reduce ripples, which are highly complex in nature. Hence in this work, keeping the structure of the DTC the same, TOA is used to select the reference flux dynamically to reduce the ripples.

With the proposed approach 59.31% reduction in torque ripple is observed which results in reduction of 36.2% battery energy consumption. In comparison to the other two techniques, the suggested algorithm exhibits superior dynamic and steady-state performance with lower torque ripple, stator current THD, flux ripple, and speed error. Additionally, it is estimated that the overall energy consumed by the motor drive for this suggested algorithm is the lowest of all since torque ripple and current THD are reduced. The performance of all three methods was compared with standard drive cycles, and the findings support the efficacy of the proposed technique. The proposed method was experimentally validated using the real-time simulator OPAL-RT 4510 with software in loop mode.

References

[1] Hou F, Chen X, Chen X, Yang F, Ma Z et al. Comprehensive analysis method of determining global long-term GHG mitigation potential of passenger battery electric vehicles. Journal of Cleaner Production 2021;289-125137. doi:https://doi.org/10.1016/j.jclepro.2020.125137

[2] Teter J. Tracking transport 2020. [Online]. Available: https://www.iea.org/topics/transport

[3] Xue M, Lin BL, Tsunemi K. Emission implications of electric vehicles in Japan considering energy structure transition and penetration uncertainty. Journal of Cleaner Production 2021;280-124402. doi: https://doi.org/10.1016/j.jclepro.2020.124402

[4] Ehsani M, Singh KV, Bansal HO, Mehrjardi RT. State of the art and trends in electric and hybrid electric vehicles. Proceedings of the IEEE 2021; 109 (6):967-84. doi: 10.1109/JPROC.2021.3072788

[5] Tabbache B, Kheloui A, Benbouzid ME. Design and control of the induction motor propulsion of an electric vehicle. In2010 IEEE Vehicle Power and Propulsion Conference 2010: (1-6). IEEE. doi: 10.1109/VPPC.2010.5729102

[6] Cho Y, Bak Y, Lee KB. Torque-ripple reduction and fast torque response strategy for predictive torque control of induction motors. IEEE Transactions on Power Electronics 2017;33 (3):2458-70. doi: 10.1109/TPEL.2017.2699187

[7] Malla M, Gudey SK, Sudha S. Transient and Steady State Characteristics of Induction Motor Drive Using DTC-SVM Technique For EV Applications. In: $11th$ International Conference on Electrical and Computer Engineering (ICECE) 2020; 403-406. doi: 10.1109/ICECE51571.2020.9393056

[8] El Ouanjli N, Derouich A, El Ghzizal A, Motahhir S, Chebabhi A, El Mourabit Y, Taoussi M. Modern improvement techniques of direct torque control for induction motor drives-a review. Protection and Control of Modern Power Systems 2019;4 (1):1-2. doi: https://doi.org/10.1186/s41601-019-0125-5

[9] Sahoo AK, Jena RK. Improved DTC strategy with fuzzy logic controller for induction motor driven electric vehicle. AIMS Electronics and Electrical Engineering 2022; 6 (3):296-316. doi: 10.3934/electreng.2022018

[10] Zaky MS. High performance DTC of induction motor drives over a wide speed range. Electrical Engineering 2015;97 (2):139-54. doi: https://doi.org/10.1007/s00202-014-0321-2

[11] Zhang Z, Wei H, Zhang W, Jiang J. Ripple Attenuation for Induction Motor Finite Control Set Model Predictive Torque Control Using Novel Fuzzy Adaptive Techniques. Processes 9 2021;9 (4):710. doi: https://doi.org/10.3390/pr9040710

[12] Savarapu S, Qutubuddin M, Narri Y. Modified Brain Emotional Controller-Based Ripple Minimization for SVM-DTC of Sensorless Induction Motor Drive. IEEE Access 2022; 10:40872-87. doi: 10.1109/ACCESS.2022.3165651

[13] Kaboli S, Zolghadri MR, Vahdati-Khajeh E. A fast flux search controller for DTC-based induction motor drives. IEEE Transactions on Industrial Electronics 2007;54 (5):2407-16. doi: 10.1109/TIE.2007.900341

[14] Subramaniam SK, Rayappan JX, Sukumar B. Fuzzy-based estimation of reference flux, reference torque and sector rotation for performance improvement of DTC-IM drive. Automatika 2022; 63 (3):440-53. doi: https://doi.org/10.1080/00051144.2022.2051966

[15] Kumar SS, Xavier RJ, Balamurugan S. Development of ANFIS-based reference flux estimator and FGS-tuned speed controller for DTC of induction motor. Automatika 2018;59 (1). doi: 10.1080/00051144.2018.1486796

[16] Depenbrock M. Direct self-control (DSC) of inverter fed induktion machine. In1987 IEEE Power Electronics Specialists Conference 1987: 632-641 IEEE. doi: 10.1109/PESC.1987.7077236

[17] Manias S. Power electronics and motor drive systems. Academic Press; 2016. ISBN: 978-0-12-811798-9

[18] Slemon GR. Modelling of induction machines for electric drives. IEEE Transactions on Industry Applications 1989;25 (6):1126-31. doi: 10.1109/28.44251

[19] Leonhard W. Control of electrical drives. Springer Science & Business Media; 2001.

[20] Sahoo AK, Jena RK. Loss minimisation of induction motor-driven electric vehicle using team-work optimisation, International Journal of Ambient Energy; 2022;43 (1):8123–8134. doi: https://doi.org/10.1080/01430750.2022.2091036

[21] Dehghani M, Trojovský P. Teamwork optimization algorithm: A new optimization approach for function minimization/maximization. Sensors 2021; 21 (13):4567. doi: https://doi.org/10.3390/s21134567

[22] Patel PD, Pandya SN. Comparative Analysis of Torque Ripple for Direct Torque Control based Induction Motor Drive with different strategies. Australian Journal of Electrical and Electronics Engineering 2022; 28:1-9. doi: https://doi.org/10.1080/1448837X.2021.2023249

[23] Maity P, Vijayakumari A. Fuzzy-Enabled Direct Torque Control for Low Torque Ripple in Induction Motors for EV Applications. In International Conference on Emerging Trends and Advances in Electrical Engineering and Renewable Energy 2020; 371-383. Springer, Singapore. doi: https://doi.org/10.1007/978-981-15-7511-2-35

[24] Ravi HK, Natesan Chokkalingam L. Current ripple reduction to improve electromagnetic torque and flux characteristics in AC drives. International Journal of Electronics 2022;109 (8):1421-42. doi: https://doi.org/10.1080/00207217.2021.1969443